J. Fluid Mech. (1980), *vol.* 96, *part* 3, *pp.* 461–479
Printed in Great Britain

On free convection experiments in inclined air layers heated from below

By DOUGLAS W. RUTH,† K. G. T. HOLLANDS AND G. D. RAITHBY

Department of Mechanical Engineering, University of Waterloo, Ontario, Canada

(Received 8 May 1978 and in revised form 11 May 1979)

The heat transfer and free convective motion, in inclined air layers heated from below, for angles of incidence $0 \leqslant \phi \leqslant 30°$, and Rayleigh numbers $100 < Ra\cos\phi < 10000$, are studied experimentally. Results of both heat-transfer measurements and flow-visualization studies are reported. The purpose of the study was to investigate the fact, first noted by Hollands *et al.* (1976), that the experimental heat-transfer data, for $\phi > 20°$, is not a function of the product $Ra\cos\phi$ only, as expected from theoretical consideration. This discrepancy between theory and experiment is here attributed to a hypothesized secondary transition in the convective motion, due primarily to perturbation velocities in the upslope direction. This secondary transition appears to be the same as that predicted theoretically by Clever & Busse (1977); qualitative agreement with their theory is observed.

1. Introduction

This paper deals with heat transfer and free convective motion, in inclined air layers heated from below, in the immediate post-conductive region. The problem configuration (figure 1) consists of a fluid layer contained between two parallel, flat, isothermal, rigid plates of extensive area, separated by a distance H, and inclined at an angle ϕ from the horizontal. The difference of temperature of the plates is ΔT; the upper plate having temperature $T_0 - \frac{1}{2}\Delta T$, and the lower plate having temperature $T_0 + \frac{1}{2}\Delta T$. A Cartesian co-ordinate system with its origin midway between the plates is constructed such that r_1, r_2 and r_3 are up the slope, across the slope and normal to the plates respectively (the corresponding fluid velocities are v_1, v_2 and v_3). The boundaries of the layer, in the r_1 and r_2 directions, are established at $r_1 = \pm L$ and $r_2 = \pm W$, where both L and W are large with respect to H. These boundaries are assumed to be adiabatic and impervious to the fluid. The flow and heat transfer of interest in the present paper are those in the central region of the plates where they are assumed to be free of the effects of these boundaries. The impervious boundaries ensure that no convection occurs between the environment and the region between the plates.

The flow and heat transfer across the layer are described by the angle of inclination ϕ, and the dimensionless groups: the Rayleigh number, $Ra = g\beta\Delta TH^3/\nu\alpha$, the Prandtl number, $Pr = \nu/\alpha$, and the Nusselt number, $Nu = qH/\Delta Tk$ (where g represents the acceleration of gravity, q the average heat flux across the central region of the layer

† Present address: Department of Mechanical Engineering, University of Calgary, Alberta, Canada T2N 1N4.

0022–1120/80/4357–8060 $02.00

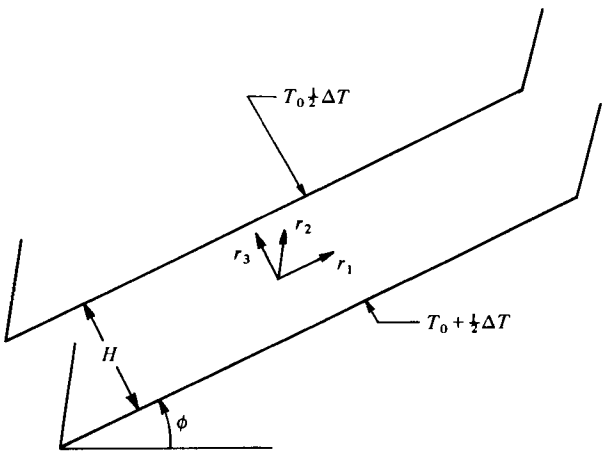

FIGURE 1. Schematic diagram of the inclined layer geometry.

far from the boundaries, and β, ν, α and k are the volumetric thermal expansion coefficient, the kinematic viscosity, the thermal diffusivity and the thermal conductivity, respectively, all evaluated at T_0). The interdependence of these parameters is described by

$$Nu = Nu(Ra, Pr, \phi). \tag{1}$$

It is well known that, provided both $Ra > 0$ and $\phi > 0$, an imbalance between pressure and gravity forces causes fluid motion to always exist. At low Ra, this motion consists of a base flow for which v_1 is cubic in r_3, and $v_2 = v_3 = 0$. The corresponding temperature is linear in r_3, yielding $Nu = 1$ or heat transfer by pure conduction (this condition is therefore termed the conduction regime). If the Ra is made sufficiently large, the base flow in the conduction regime becomes unstable. Birikh *et al.* (1968) and Gershuni & Zhukhovitskii (1969) showed by a stability analysis that the incipient flow at this instability point must consist of rolls [with their axes in either the r_1 direction (termed longitudinal rolls) or the r_2 direction (termed transverse rolls)] and never three-dimensional cells. For $\phi < \phi_c$, where ϕ_c is a characteristic angle dependent on Pr ($\phi_c \simeq 88°$ for water, $Pr \simeq 7$ and $\phi_c \simeq 71°$ for air, $Pr \simeq 0{\cdot}7$), longitudinal rolls were predicted to be more unstable, and hence to be the expected incipient mode. The critical condition defining the state of marginal stability of the conduction regime was given in terms of a critical Rayleigh number, and it was shown that, if instability resulted in longitudinal rolls, then

$$(Ra \cos\phi)_c = 1707{\cdot}762. \tag{2}$$

Equation (2) would therefore correspond to the critical condition provided $\phi < \phi_c$. Most of these results were theoretically confirmed by Hart (1971*a*) and Unny (1972).

Visual experimental confirmations of longitudinal rolls have been reported by several authors. Kursweg (1970) confirmed longitudinal rolls as the preferred mode of convection for $\phi < 75°$ and $Pr \simeq 500$. The critical condition was roughly consistent with (2). Malinov (1971) reported confirmation of longitudinal rolls in glycerine ($Pr \simeq 1000$) for $\phi < 75°$ but did not compare his results with (2). Hart (1971*a*) reported results for water, confirming both the existence of longitudinal rolls and agreement

within experimental uncertainty with (2). De Graaf & Van der Held (1953), using air as the fluid and injecting smoke to make the convection patterns visible, observed longitudinal rolls at $\phi = 10°$ and 20° only. For $30° \leqslant \phi \leqslant 60°$, the layer was observed to be 'turbulent' after transition, in apparent contradiction with the stability theory which predicts steady motion. It is of interest to note that their longitudinal rolls at $\phi = 10°$ and 20° were observed to have the fluid 'spiral upward along the circumference of the rolls and come back through the centre'.

When convective motion initiates, the heat transfer can be expected to increase and Nu departs from unity. Using this principle, Hollands & Konicek (1973) confirmed the critical Rayleigh number predicted by (2) using air as the fluid. However, the magnitude and form of the rise of Nu with Ra immediately after instability were not as expected, as was pointed out by Hollands *et al.* (1976). The basis for the expected form and magnitude of the post-stability rise of Nu with Ra is a theory of Clever (1973) and its extension by Hollands *et al.* Provided that the upslope derivatives $(\partial/\partial r_1)$ of temperature and velocity are zero, this theory demonstrates that the Nusselt number, rather than being a function of Ra and ϕ separately, is a function only of the product $Ra\cos\phi$. Equation (1) may then be replaced by

$$Nu = Nu(Ra\cos\phi, Pr). \tag{3}$$

The existence of longitudinal rolls implies $\partial/\partial r_1 = 0$; therefore, since the stability analysis predicts longitudinal rolls for $0° < \phi < \phi_c$, (3) is expected to apply in the immediate post-conductive regime for $0° < \phi < \phi_c$. For the purpose of brevity, if (3) applies, it will be said that the heat transfer 'scales' or that 'scaling' occurs. Although Hollands *et al.* (1976) determined scaling for data at 0° and 15°, departures from scaling in the immediate post-conductive regime of up to 35 % were observed for $\phi = 30°$ and 45°. A return to scaling was noted for $Ra\cos\phi > 4 \times 10^4$ at both these angles.

The consistency between the heat transfer results of Hollands *et al.* (1976) and the flow visualization results of De Graff & Van der Held (1953) should be noted. Both results are consistent with longitudinal rolls existing for $\phi < 25°$ but not, contrary to stability theory, for $\phi > 25°$. A possible explanation for this behaviour would appear to be the breakdown of the longitudinal rolls by a secondary instability at a Rayleigh number only slightly in excess of the critical Rayleigh number for the primary instability. For such a secondary instability to be consistent with currently accepted observations, it would have to have the following characteristics:

(1) it must not occur for $Pr \simeq 7$ (water);

(2) it must not occur for $Pr \simeq 0{\cdot}7$ (air) provided $\phi < \sim O(25)°$;

(3) it must occur at Ra only slightly greater than $1708/\cos\phi$ for $\phi > \simeq 25°$;

(4) its superposition with the longitudinal rolls of the primary instability must be a flow that appears 'turbulent';

(5) (and perhaps most curious) it must produce a decrease, rather than the usual increase, of heat transfer.

The present paper describes work aimed at experimentally examining the above phenomena, testing the hypothesis of a secondary instability and, if accepted, exploring the nature of this instability. Concurrent with the completion of this work, a study by Clever & Busse (1977) appeared in the literature. Based on a theoretical stability analysis, Clever and Busse predicted the existence of a secondary instability,

which, for air and $\phi > 20°$, occurs at values of Ra only slightly above 1708. Furthermore, they predicted that this instability, in some cases, did not persist as Ra was increased, but was actually stabilized, causing a return to the longitudinal roll form. It will be seen later in the present paper that this is, qualitatively, the behaviour observed in inclined air layers. The current work was performed independently of that of Clever & Busse (1977), and was motivated by the heat transfer aspects of the problem more than the flow stability *per se*.

2. The heat transfer measurements

The purpose of the heat transfer measurements was first, to delineate more precisely the angle below which scaling applies and above which it does not and, second, to examine in detail the Nu–Ra behaviour, after the first instability, for indications of a secondary instability. To this end, precise results, at small increments in Ra and ϕ, were obtained.

The experiments were carried out on the same apparatus as used by Hollands & Konicek (1973) and Hollands *et al.* (1976). In this apparatus, the flat plates of figure 1 are made of 1 cm thick copper, with lateral dimensions $L = 28$ cm and $W = 30{\cdot}5$ cm. The heat transfer is measured over the region

$$-6{\cdot}45 \text{ cm} \leqslant r_1 \leqslant 6{\cdot}35 \text{ cm}, \quad -6{\cdot}35 \text{ cm} \leqslant r_2 \leqslant 6{\cdot}35 \text{ cm}$$

of the lower plate, by means of a separate electrically heated plate, using a method which is essentially a guarded hot plate technique (for details see Hollands & Konicek 1973). The temperature difference, ΔT, was made approximately 10 K by means of two differentially heated streams of water (from two separate constant temperature baths) circulated through banks of tubes soldered to the back surfaces of the plates. The average temperature was approximately 300 K.

It can be estimated from boundary-layer calculations, that the effects of the boundaries at $\pm L$ do not penetrate to the region where heat transfer is measured, provided $\phi < 60°$. To further check the effect of these boundaries, the spacing H used in the present experiments ($H = 1{\cdot}90 \pm 0{\cdot}01$ cm) was made different from that of the earlier experiments ($H = 1{\cdot}27$ cm). Presuming the effects of the boundaries will depend on the ratio L/H, the effects may be assumed small if the dimensionless results are essentially the same for the two experiments. The effects of the boundaries at $\pm W$ are expected to be less important than those at $\pm L$. In the present study, heat transfer measurements were made for $10^2 < Ra < 10^4$ and for $\phi = 0°$, 5°, 10°, 15°, 20°, 25°, 27·5° and 30°. The angles $\phi = 0°$, 15° and 30° are in common with the previous study of Hollands & Konicek (1973).

The heat transfer data will be presented in the form of plots of Nu *vs.* $Ra\cos\phi$ (or its inverse). If scaling occurs, the results for different angles should fall along the same curve. In addition, the data will be compared with the equation

$$Nu = 1 + \Gamma[1 - (Ra\cos\phi)_c/Ra\cos\phi]. \tag{4}$$

This equation is obtained by scaling the equation for heat transfer in a horizontal fluid layer in the immediate post-conduction regime, derived by means of the power integral method by Nakagawa (1960) and Malkus & Veronis (1958), and given by

$$Nu = 1 + \Gamma(1 - Ra_c/Ra). \tag{5}$$

The value of Γ is obtained theoretically as 1·441 (Platzman 1965; Hollands 1965). Equation (3) implies that, if longitudinal rolls are the preferred form of convection, then (5) may be rewritten, for inclined layers, as (4). Equation (4) has been verified experimentally by Hollands *et al.* (1976), for $\phi = 0°$ and 15° and $1708 \leqslant Ra \leqslant 5000$. Above $Ra \simeq 5000$, the assumptions used in the derivation of (5) are presumably no longer valid.

Figure 2 shows a comparison between the present results for $\phi = 0°$, 15° and 30° and those of Hollands (1967) ($\phi = 0°$ only, H in the range 1·27 cm to 5·08 cm) and Konicek (1971).† The agreement is very good, with the present results showing less scatter than either of the previous sets. The agreement between the various data sets may be interpreted as verification that boundary effects at L and W do not penetrate to the region where heat transfer is measured.

Results for $\phi \leqslant 15°$

Figure 3 presents the data for $\phi = 0°$, 5°, 10° and 15°. It is noted that, although the data for $\phi = 5°$, 10° and 15° indeed scale, the $\phi = 0°$ data lie noticeably below the other data. The reason for this slight non-scaling of the $\phi = 0°$ data is not clear; however, the good agreement between the $\phi = 5°$, 10° and 15° data, coupled with the exceptionally good agreement between these data and (4) for $Ra\cos\phi < 3500$, is interpreted as confirmation of scaling. For $Ra\cos\phi > 3500$, the data rise steadily above the equation, making the equation in error by approximately 10 % at

$$Ra\cos\phi = 10000.$$

Results for $\phi \geqslant 20°$

Figure 4 presents the results for $\phi = 20°$, 25°, 27·5° and 30°, with the $\phi = 5°$ data included for comparison. The abscissa is the inverse of $Ra\cos\phi$ and the straight line represents (4). Whereas the $\phi = 5°$ data agree well with the line, the $\phi = 20°$ data show a marked suppression in heat transfer, beginning very near $Ra\cos\phi = 1708$, and continuing until $1/(Ra\cos\phi) \simeq 4 \times 10^{-4}$ ($Ra\cos\phi \simeq 2500$). Above $Ra\cos\phi \simeq 2500$, the $\phi = 20°$ data agree reasonably well with the line. The $\phi = 25°$ data show a more pronounced Nu suppression than the $\phi = 20°$ data, but at $1/(Ra\cos\phi) \simeq 3{\cdot}3 \times 10^{-4}$ ($Ra\cos\phi \simeq 3000$) the data again approach the $\phi = 5°$ data. The $\phi = 27{\cdot}5°$ and 30° data show mutually similar behaviour, with greater suppression than the $\phi = 25°$ data. In no place do these data agree with the line and scaling is not re-established until $1/(Ra\cos\phi) \simeq 1 \times 10^{-4}$ ($Ra\cos\phi = 10000$).

Statistical analysis of the heat transfer data

In order to statistically analyse the heat transfer suppression, equation (4) was fitted to the data, using a least squares method, with $(Ra\cos\phi)_c$ and Γ as fitting parameters. Data for the range $1708 \leqslant Ra\cos\phi \leqslant 2250$ (the region immediately after the onset of instability) were used. The results are presented in table 1. Also tabulated are the number of points, N, used in the fit and the standard deviation of the residuals, σ. The uncertainty limits on Γ and $(Ra\cos\phi)_c$ are based on 95 % confidence limits. All

† The original results of Konicek contained a small calibration error; figure 2 shows corrected values.

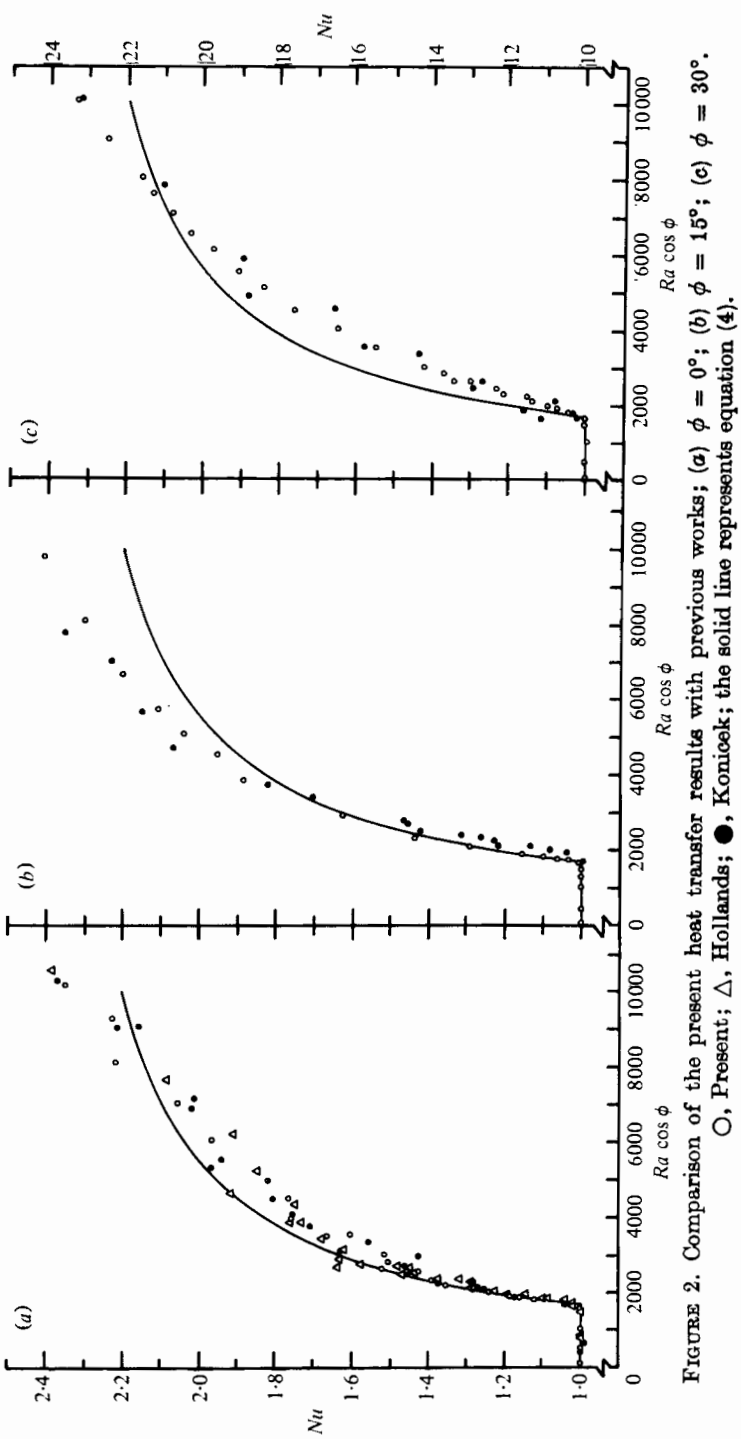

FIGURE 2. Comparison of the present heat transfer results with previous works; (a) $\phi = 0°$; (b) $\phi = 15°$; (c) $\phi = 30°$. ○, Present; △, Hollands; ●, Konicek; the solid line represents equation (4).

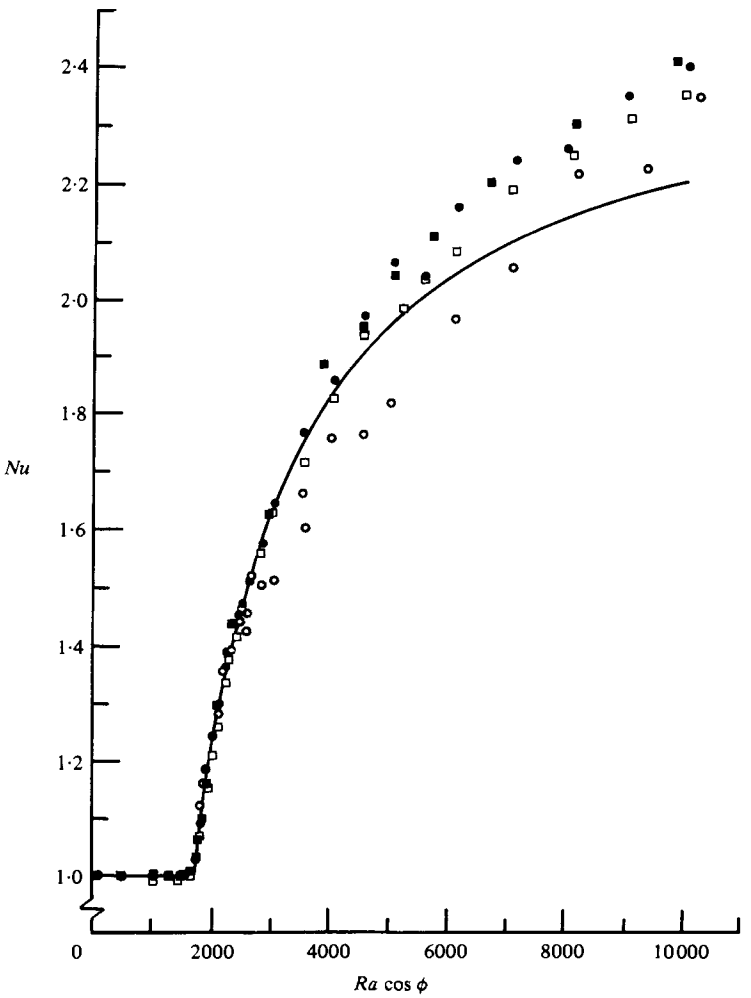

FIGURE 3. Heat transfer results ($\phi \leqslant 15°$): ○, $\phi = 0°$; ●, $\phi = 5°$; □, $\phi = 10°$; ■, $\phi = 15°$; the solid line represents equation (4).

the values of $(Ra\cos\phi)_c$ agree with the theoretical value, 1708, to a tolerance well within the uncertainty. For $\phi = 5°$, 10° and 15°, the values of Γ agree with the theoretical value of 1·441; the value for $\phi = 0$ is, however, slightly low. These results show that the data for $\phi = 0°$ statistically disagree with the equation and that these data are anomalous; no satisfactory reason for this anomaly is known.

The data for $\phi \geqslant 20°$ all yield values of Γ which lie below 1·441 by a statistically significant amount. The statistical analysis therefore indicates suppression of the heat transfer in the immediate post-conduction regime for $\phi \geqslant 20°$.

From considerations of the experimental errors involved in the experiment, it was estimated that $Ra\cos\phi$ and Nu could be determined to within ± 100 and $\pm 0{\cdot}04$ respectively. These values are consistent with the standard deviations reported in table 1.

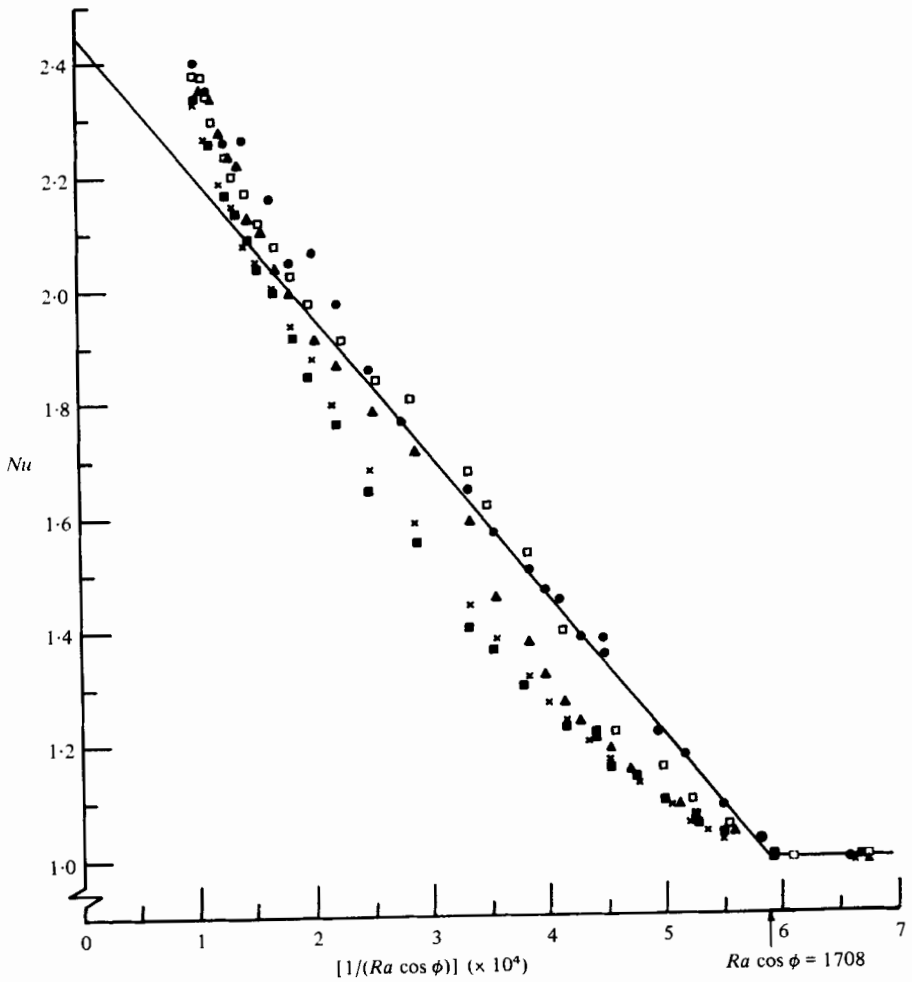

FIGURE 4. Heat transfer scaling determination: ●, $\phi = 5°$; □, $\phi = 20°$; ▲, $\phi = 25°$; ×, $\phi = 27{\cdot}5°$; ■, $\phi = 30°$; the solid line represents equation (4).

Angle (degrees)	Γ	$(Ra\cos\phi)_c$	σ	N
0	$1{\cdot}302 \pm 0{\cdot}121$	1663 ± 239	0·01118	6
5	$1{\cdot}514 \pm 0{\cdot}156$	1703 ± 270	0·01661	7
10	$1{\cdot}442 \pm 0{\cdot}044$	1740 ± 82	0·00277	5
15	$1{\cdot}436 \pm 0{\cdot}071$	1687 ± 124	0·00485	8
20	$1{\cdot}070 \pm 0{\cdot}125$	1713 ± 299	0·00841	5
25	$0{\cdot}802 \pm 0{\cdot}144$	1712 ± 474	0·00850	4
27·5	$0{\cdot}808 \pm 0{\cdot}057$	1762 ± 187	0·00378	6
30	$0{\cdot}705 \pm 0{\cdot}130$	1720 ± 482	0·00864	6

TABLE 1. Statistical analysis of the heat transfer data ($1708 \leqslant Ra\cos\phi \leqslant 2250$).

3. The flow visualization experiments

An apparatus was constructed in order to study visually the forms of convection for $1700 \leqslant Ra \leqslant 10000$. The apparatus (figure 5) consisted of an insulating enclosure, a heated plate, an enclosing frame and a cooled plate. The insulating enclosure contained 15·3 cm of polystyrene to reduce back losses and thereby help to ensure an isothermal plate. The heated plate was constructed of 1·9 cm aluminium, with 14 thermofoil heaters bonded to its lower side. The heaters were controlled by an on–off temperature controller, using a thermistor mounted to the plate as its sensor. Six copper–constantan thermocouples were embedded in the plate to measure the temperature of its upper surface. The enclosing frame, made of 3·8 cm wide Plexiglas, provided a transparent, impervious boundary at $L = \pm 35{\cdot}6$ cm and $W = \pm 28{\cdot}0$ cm. The depth of the frame was 2·0 cm (i.e. $H = 2{\cdot}0$ cm). The cooled plate consisted of three components, a 1·9 cm Plexiglas lower plate, a 0·6 cm water passage and a 0·6 cm Plexiglas cover plate. Temperature-controlled water was passed between the two Plexiglas plates to maintain the lower plate at a constant temperature. Six thermocouples were mounted on the lower face of the lower plate to sense its temperature. The entire apparatus was inclined by means of hinges which fixed the insulating enclosure to a table. The apparatus was held in place by two retaining bars with a screw mechanism provided to aid in changing the angle. The angle was accurately measured using a tilting level.

Sets of O-rings were located between the heated plate and the enclosing frame, and between the enclosing frame and the cooled plate. In this manner, the enclosed fluid layer became a sealed chamber allowing the working fluid to be pressurized. For safety and to prevent excess deflexion of the cooled Plexiglas plate, reinforcement was provided by two 2×2 in. aluminium angles. In order to ensure thermal isolation of the two plates, all connecting bolts were passed through oversized holes in the plates and frame, and further, through oversized holes in two Plexiglas insulating spacers. The bolts were located in the centre of the holes by means of washers, attached to an aluminium angle, which was in turn attached to the insulating spacers. The apparatus was constructed as a pressure chamber in order to accomplish changes in Ra by changes in pressure (i.e. density). In the results described below, this feature was not used, Ra being varied by varying ΔT.

The convection patterns were visualized by introducing cigar smoke, through ports in the enclosing frame, by means of a variable speed tube pump. Smoke could be introduced at four points along the hinged end of the apparatus and two points at the opposite end. Viewing was possible through the cooled plate, as well as along all four edges. Lighting was by means of a Spectra-Physics Stabilite Model 120 Helium–Neon Laser, with the beam expanded to 50 mm diameter. By mounting an optical slit in front of the expander lens, 'slices' through the layer could be illuminated. By turning the slit, the orientation of the slices could be changed. The laser beam expander assembly was mounted on an omni-directional tripod. By suitable adjustment, the tripod became a mechanism that allowed the observer to sweep the beam throughout the layer. Photographs were taken using a 35 mm SLR camera and 1600 ASA film. Exposure times, at an aperture of f 1·4, were typically 15–20 s. Since ambient light would have precluded these long exposures, the entire apparatus was enclosed in a 'light tight' black polyethylene tent.

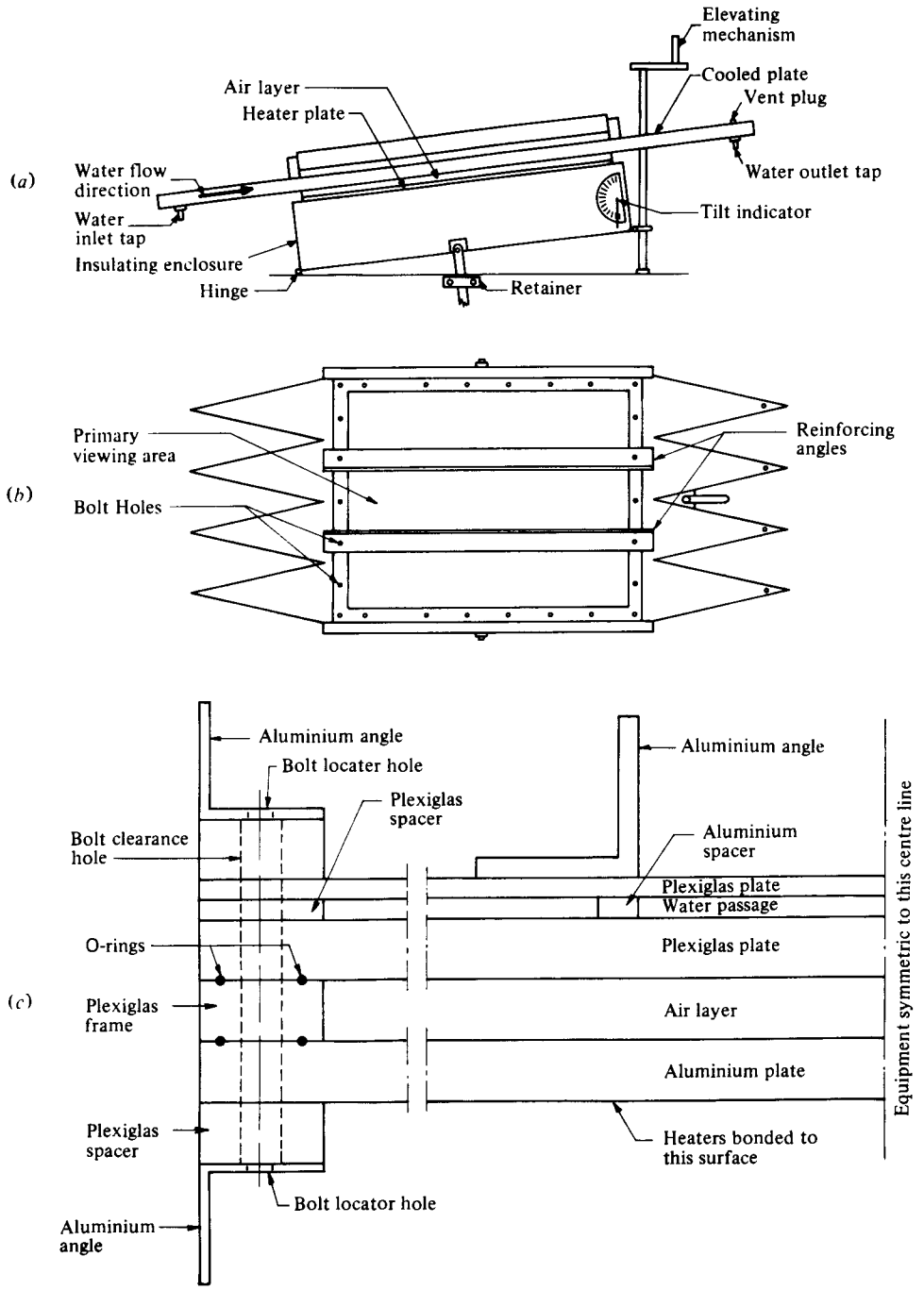

FIGURE 5. Schematic diagram of the equipment: (*a*) side view; (*b*) plan view; (*c*) cross-section.

Two different studies were performed: the first, a study of the convective form over a range of Ra's and ϕ's (with observations in planform, mainly using the full laser beam), and the second, a more detailed study over a range of Ra's at $\phi = 15°$ (with observations in planform and cross-section, mainly using the optical slit). For these studies the error in determining the Ra was estimated at $\pm 5\%$. In addition, the cyclical control of the heated plate caused a variation in the Ra with a range of less than 75. The error in angle determination was less than 0·25° in all cases.

The convective form studies

The studies to determine the form of the convective motion all followed a similar format. An initial ϕ (generally $\phi = 15°$) and a particular Ra were chosen and the equipment was allowed to stabilize (typically for 5 to 12 hours). Smoke was then introduced and a settling time of 20 to 30 minutes was allowed, to permit the disturbances to decay, before observations and photographs were taken. The angle was then changed and a settling time of 5–10 min was allowed before taking new observations and photographs. No new smoke was introduced after this angle change. This technique overcame the problem of possibly confusing smoke injection effects with inherent unsteadiness of the convection. Transition points, between steady and unsteady regimes, were determined by changing the angle of inclination (while holding the Ra constant) long after all injection-related transients had decayed. In addition, the screw mechanism allowed for smooth variations in the inclination angle, minimizing possible vibrational disturbances during the movement of the layer.

Figures 6 to 9 (plates 1 to 4) show the planform photographs of the convective motion for a range of Ra and ϕ. The dark bands running down either side of the photographs are two spacer rails, located between the layers of Plexiglas in the cooled plate, and running in the upslope direction. These rails are 15·25 cm apart. The wires visible in some photographs are thermocouples; the shadows are due to bolts.

As was expected, for Ra and ϕ sufficiently small (but $\phi \neq 0$), steady rolls with their axes approximately in the upslope direction were observed (see figure 7*c*). At very low Ra and ϕ, steady rolls with a bend in their axes were observed (figure 6*b*). This bend extended in a single arch for the full length of the apparatus. This feature was termed 'bent rolls'. In some other cases, rolls having a waviness in their axes (figure 6*c*) were observed (the wavelength was of order 15 cm). These rolls showed no time-dependent (unsteady) behaviour. This feature was termed 'wavy rolls' or 'waviness'. Rolls with two types of unsteadiness were observed. One was a gentle lateral swaying. This feature was termed 'lateral motion'. The other was a motion whereby a roll would break into two segments, the bottom or both segments would turn down forming an open loop, then the loops would break up and longitudinal rolls would be temporarily restored. The time scale of this motion was several seconds. This feature was termed 'looping'. The wavy rolls observed here appear to have many features in common with those observed by Hart (1971*b*) in water. The major difference between the occurrence of this phenomenon in air and in water is that it initiates at different values of Ra and ϕ.

In cases where unsteady motion was observed, the persistence of visual flow patterns was much reduced. If, when the angle was changed, the new position corresponded to a case where the convection was steady, the change in angle produced little observable change in the intensity of the smoke patterns. If, however, the new

position corresponded to a case where the convection was unsteady, the smoke patterns would be barely visible or totally diffused by the end of the five minute settling period. This behaviour served as a very sensitive measure for the existence of steady convection at any given Ra and ϕ.

Although the rolls became very unsteady at high Ra and ϕ, it must be made clear that there was always an underlying longitudinal roll form. If, at the end of the 5 minute settling period, all the smoke was diffused, a new supply of smoke was injected. Upon introduction, the smoke always showed a roll structure. Unsteadiness was clearly manifest; however, a fundamental laminar roll structure was always evident.

When the smoke was introduced at the hinged end of the apparatus, it first formed what appeared to be a series of connected handwritten U's with their open ends in the upslope direction. The tails of the U's would then break, forming two rolls in the bowl of each U. The left-hand roll of the two tended to contain more smoke than the right-hand roll, producing an alternate dark–light pattern in the rolls which often persisted well after settling had occurred (see figures 6*b* and 9*c*, *d*). The reason for this is not known. Also, when the smoke was first introduced, it always disturbed the existing convection patterns. As the flow restabilized, the smoke was trapped in certain positions, creating what appeared to be a great deal of internal detail in the rolls (e.g. figure 8*a*). In some cases (e.g. figure 7*d*), these features seemed to indicate that the rolls were separated, being made up of a series of linked rolls. However, observations of the flow pattern of individual smoke particles showed this was not the case. These internal details were concluded to be the result of the pattern of smoke trapped during the unsteadiness caused by smoke introduction. In the cases where steady rolls were eventually formed, these details persisted without discernible change for 30 minutes or longer.

At $\phi \leqslant 15°$ the motion described by De Graff & Van der Held (1953) (i.e. flow spiralling up the outside of the roll and down the core) was observed, but only immediately after smoke was introduced. After 15–20 min, all evidence of such motion had disappeared. De Graff & Van der Held's observations have, therefore, been ascribed here to disturbances resulting from the injection of smoke. The present technique permitted observation well after the initial effects of smoke introduction had settled out. In fact, some observations of steady rolls were made up to four hours after smoke injection. The observation of 'turbulence' by De Graff & Van der Held above $\phi = 30°$ was also not well confirmed. As noted above, an underlying laminar roll structure was evident in even the most unsteady cases considered in the present study. These more detailed results, obtained in the present work, can undoubtably be attributed to the use of laser lighting.

The detailed observations, at each Ra studied, are presented in the appendix. Figure 10 summarizes these observations by outlining the regimes where the various motions were observed. Three regimes exist: the steady but bent rolls, the steady straight rolls and the unsteady rolls. The wavy rolls were observed in the region just above the curve separating the steady and unsteady regions, and in the range $1708 \leqslant Ra \cos\phi < 3000$. It is of interest to note that at some angles, such as $\phi = 20°$, the initial transition from pure base flow is to an unsteady motion; at higher Ra, however, these rolls become steady rolls while, at still higher Ra, they become unsteady again.

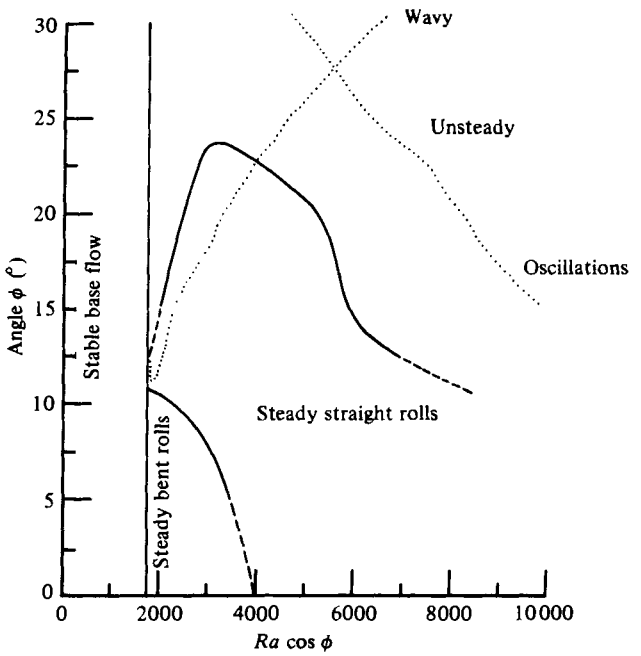

FIGURE 10. Regimes of motion: ——, present experiments; ·····, theory of Clever & Busse (1977).

The theoretical results of Clever & Busse (1977) are also plotted on figure 10. For $\phi > 12{\cdot}5°$ the left branch of the wavy instability line essentially coincides with the vertical line separating the stable base flow regime and the unsteady regime. Their prediction of a secondary transition is, therefore, well confirmed. The right branch of the wavy instability indicates a return to a stable regime. The region between and below the 'wavy' and 'oscillation' lines should therefore correspond to a stable regime. Although the theoretical results are in qualitative agreement with the experimental observations, quantitative disagreements of approximately 50 % occur in the $Ra \cos \phi$ location of the curves. In discussing their comparison with Hart's data, Clever & Busse (1977) suggested that the disagreement there resulted from the time delay for the instability to become visible. This is unlikely to be the reason for the present disagreement since the instabilities in air set in much more rapidly.

By counting the number of rolls in figures 6–9, and noting that the spacing between the rails is 15·25 cm and the depth of the layer is 2·0 cm, the spatial wavenumber, a, of the rolls may be determined. For the steady situations, and $Ra < 4000$, approximately $7\frac{1}{4}$–$7\frac{1}{2}$ rolls were found between the rails, corresponding to the value

$$2{\cdot}98 \leqslant a \leqslant 3{\cdot}09.$$

This agrees well with the theoretical value of the critical spatial wavenumber, $a_c = 3{\cdot}117$. The steady rolls above $Ra = 4000$ had $a \simeq 2{\cdot}6$, while the unsteady rolls above $Ra = 4000$ had $a \simeq 3{\cdot}7$.

Detailed results for $\phi = 15°$

Extensive studies were performed at $\phi = 15°$ to determine the details of the structure of convective motion over a range of *Ra*'s. These studies were performed using the optical slit. Details of the motion were observed in planes of four basic orientations. With the slit parallel to the plates, observations were made near the heated plate (bottom of the fluid layer), midway between the plates (centre) and near the cooled plate (top). The slit was also oriented perpendicular to the plates, to observe the rolls in cross-section. It was found most satisfactory to observe the smoke patterns with the eye at an angle of approximately 30° from the laser beam. At this angle, individual smoke particles were clearly visible. However, to ensure that the whole field of view was in focus, all photographs were taken at an angle of 90° to the laser beam.

Figure 11 (plates 5, 6) shows photographs of the cross-sections of the rolls, illuminated with the slit perpendicular to the plates. In all pictures the upper part is the reflected image of the rolls in the upper Plexiglas plate. The $Ra \simeq 1925$ photograph (figure 11*a*) shows rolls of uneven size and considerable variation in detail. The $Ra \simeq 2370$ photograph (figure 11*b*) shows very regular well-defined rolls. From the more extensive visual observations, it was determined that the transition from uneven-sized rolls to even-sized rolls occurred between $Ra \simeq 2100$ and $Ra \simeq 2300$. Figures 11(*c*) and 11(*d*) ($Ra \simeq 2625$ and $Ra \simeq 2950$ respectively) again show regular roll patterns; however, the rolls have skewed interiors (note particularly the 7th roll from the right-hand side in figure 11*c* and almost every roll in figure 11*d*). At $Ra \simeq 3870$ (figure 11*e*), regular rolls are still evident and indications of skewing persist; however, the width of the rolls has increased noticeably. The roughly square rolls of previous *Ra*'s are now clearly rectangular. By $Ra \simeq 5080$ (figure 11*f*) the rolls are becoming of uneven size.

The results of figure 11 confirm the convective form study. The wavy rolls at $\phi = 15°$ and $Ra \simeq 1925$ are manifest as rolls of uneven size in cross-section. At $\phi = 15°$ and $Ra \simeq 5000$, stable rolls were observed in plan-form, while at $Ra \simeq 5800$ there were clear signs of lateral motion. The size unevenness noted in figure 11(*f*) can probably be attributed to this transition.

Observations over the range $1900 < Ra < 7000$ were performed with the slit parallel to the plates. Photographs were not generally possible in this case, since the observer tracked individual smoke particles which did not scatter enough light to be recorded photographically. Figure 12 summarizes the observations, in plan view and cross-section, of two rolls, for $2000 < Ra < 2500$. Figure 12(*d*) shows the locations of the three planes of figure 12(*a*), (*b*) and (*c*), and indicates the location of the 'interfaces' described below. Near the top of the layer (figure 12*a*), smoke particles emerged from the outside interfaces, proceeded straight across the two rolls, then turned (downward in plan view), appearing to flow almost parallel to the centre interfaces. These features were very easily observed, with the interfaces clearly discernible. Near the centre of the layer (figure 12*b*), interfaces were more difficult to identify because there was little evidence of cross-roll motion. The interfaces clearly seemed to move at approximately the same speeds, in alternating directions, with the centre of the rolls remaining roughly stationary. Near the bottom of the layer (figure 12*c*), the interfaces were once more clearly identified. Here the smoke particles

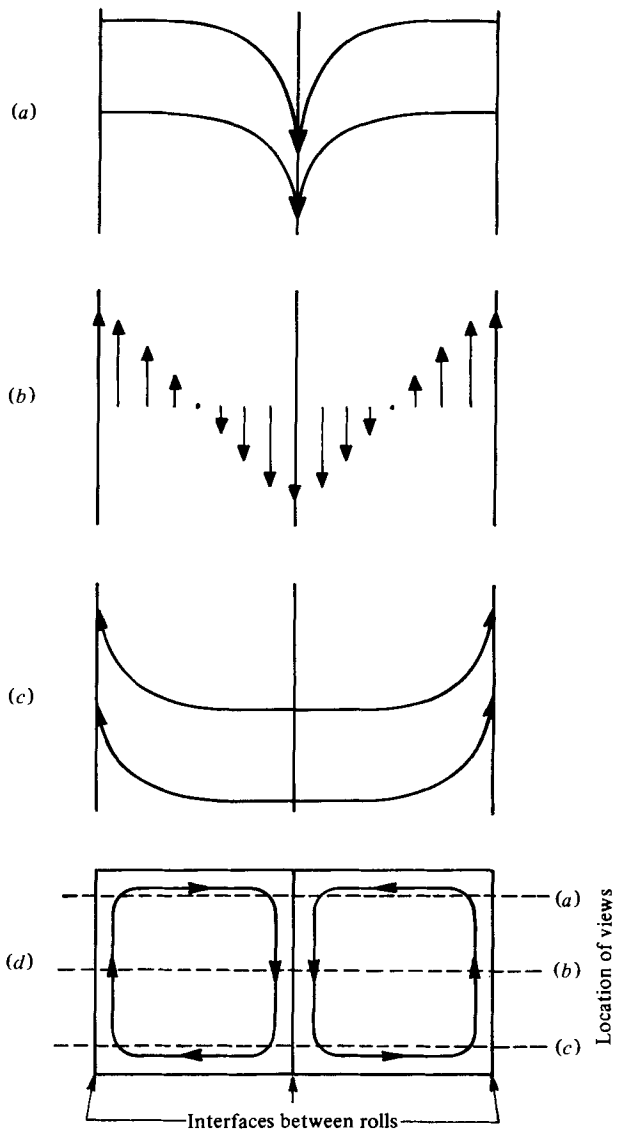

FIGURE 12. Flow patterns at $2000 < Ra < 2500$: (*a*) near top of layer (plan view); (*b*) near centre of layer (plan view); (*c*) near bottom of layer (plan view); (*d*) nomenclature (end view).

emerged from the centre interface, proceeded across the two rolls, then turned (this time upward in plan view), to flow parallel to the outside interfaces. At higher Ra ($Ra \simeq 3000$) the pattern near the top of the layer was almost U-shaped, with particles coming up the outside interfaces crossing over the rolls in two arcs and flowing down the centre interface. Near the bottom the opposite pattern was observed.

The observations reported for the parallel slit experiments are necessarily confined to the region of steady rolls, with the flow consisting of the superposition of the roll structure on the base flow. The striking feature of the observations is the magnitude of

the upslope velocity associated with the rolls (v_{1r}). Since the upslope velocity associated with the base flow (v_{1b}) is not a function of r_2, it follows that the variation of v_1 observed in figure 12 is due to v_{1r}. At $Ra \simeq 2500$, v_{1r} is clearly of the same order of magnitude as v_{1b}, while observations at $Ra \simeq 3000$ would indicate that, at higher Ra, v_{1r} would exceed v_{1b}. The existence of v_{1r} is not inconsistent with the theoretical requirement for scaling (provided $\partial v_{1r}/\partial r_1 = 0$), nor is it inconsistent with the stability theory. In fact, its existence was first indicated by Birikh *et al.* (1968) based on their stability study.

From measurements on figure 11, the spatial wavenumber for the roughly square rolls ($Ra \simeq 2380$ and 2950) was found to be $a \simeq 3{\cdot}14$. This is in excellent agreement with the results from figures 6–9, as well as stability theory. At $Ra \simeq 3870$, when the rolls become rectangular, $a \simeq 2{\cdot}62$. Again this result is in excellent agreement with the previous results.

Comparison with the heat transfer measurements

The flow visualization results correlate well with the heat transfer results. In situations where steady rolls (either straight or bent) were observed, the heat transfer data scaled. When unsteadiness was observed, the heat transfer data did not scale. This is clearly shown for $\phi = 20°$ in figure 13 (plate 7), where the patterns are correlated with the heat transfer results. At the point $Ra\cos\phi = 2280$, where waviness was observed but a photograph was possible, the heat transfer data almost scales. At $Ra\cos\phi = 1810$, where the heat transfer data are clearly suppressed, the pattern is so unsteady as to preclude photographing. In addition, the point where the heat transfer data begin to depart from (4) ($Ra\cos\phi \simeq 4000$), appears to be associated with a change in spatial wavenumber from $a \simeq 3{\cdot}05$ to $a \simeq 2{\cdot}58$.

It should be noted that the heat transfer scales when the rolls are bent, provided they are steady. Clearly, bent rolls cannot strictly satisfy the condition, $\partial/\partial r_1 = 0$, necessary for scaling. Presumably, the deviation from scaling associated with the noted small degree of bending is not sufficient to alter the heat transfer. The present experiments confirmed that the bent rolls were repeatable. However, an explanation of their cause must await further experimentation. Their occurrence was concluded to be unimportant to the present problem.

4. The secondary instability hypothesis

The results of the present study are consistent with the hypothesis of the existence of the instability, with respect to the longitudinal roll flow pattern, described in the introduction. Since the longitudinal rolls themselves result from an instability, the primary instability, this further instability will be termed the secondary instability. An alternative hypothesis is that the primary instability is time-unsteady with a temporal variation magnitude which is small at Ra near the critical value, but increases with increasing Ra. However, the observed persistence of the steady longitudinal roll pattern, and the rather sudden transition to unsteady flow over an angle change of only a few degrees, appear to argue strongly against this hypothesis. Also not in support of this idea are the analytical (stability theory) prediction that the primary instability is time independent and the excellent experimental verification of the Ra_c predicted by stability theory.

On the basis of the secondary instability hypothesis, figure 10 may be interpreted as a mapping of the regions in the Ra–ϕ plane for which the longitudinal rolls are stable to time-dependent disturbances. A search in figure 4 for a secondary change in slope of the heat transfer curve, for any particular ϕ, reveals only that, if such a transition exists, it occurs close enough to $Ra\cos\phi = 1708$ to preclude detection. This would suggest that the critical condition for the secondary instability is in the range $1708 < (Ra\cos\phi)_{c_2} < 1750$. Consideration of a possible mechanism for the secondary instability must take into account the v_{1r} velocity associated with the longitudinal rolls. The magnitude of this velocity grows with both Ra and ϕ and, at sufficiently high Ra and ϕ, may become subject to a shear instability. Perhaps this is the secondary instability observed. A point which should be kept in mind is that, for the angles $\phi = 20°$ and 25°, the heat transfer data and the flow visualization both indicate a temporary suppression of this secondary instability for an intermediate range of Ra. This is manifest by a return to agreement between (4) and the heat transfer data, and the visual observation of steady rolls.

5. Conclusions

(1) The present work has confirmed and extended the earlier work of Hollands *et al.* (1976) on heat transfer in inclined layers. The scaling law has been established for $5° \leqslant \phi \leqslant 15°$, while the $\phi = 0°$ data appears to be significantly anomalous. For $\phi > 20°$, the heat transfer does not scale near the critical Rayleigh number; however, scaling is re-established at higher Ra. The value of Ra above which the data scale increases with increasing ϕ.

(2) For $\phi \leqslant 15°$, the generalized Malkus–Veronis–Nakagawa equation (4) predicts the heat transfer very well for $Ra\cos\phi < 3500$ and adequately up to $Ra = 5000$. For $\phi = 20°$ and 25° the Nusselt number is below that predicted by the equation, until $Ra\cos\phi$ reaches a sufficiently high value.

(3) The existence of steady longitudinal rolls for low Ra and ϕ was confirmed. However, at certain Ra and ϕ (summarized in figure 10) the steady rolls are replaced by unsteady flow patterns. The theoretical results of Clever & Busse (1977) have been shown to qualitatively agree with the flow visualization results.

(4) The flow visualization results of De Graff & Van der Held were confirmed only in the sense that longitudinal rolls were not the observed convective form for $\phi > 20°$. However, their detailed results were not confirmed. This disagreement has been attributed to the increased illumination provided by the use of laser lighting, which allowed a greatly extended viewing time in the present work.

(5) Flow visualization observations in the steady roll region showed a highly significant spatially periodic component of velocity in the upslope direction. At $Ra \simeq 2500$, its magnitude is of the same order as that of the base flow, while for increased Ra its magnitude exceeds that of the base flow.

(6) Measurements of the spatial wavenumber, in the region of steady rolls and $Ra\cos\phi < 5000$, agree well with the value predicted by stability theory. Above $Ra = 5000$, if the rolls were steady, the spatial wavenumber tended to decrease. This decrease appears to be associated with a disagreement between the heat transfer data and (4). In cases of incipient unsteadiness, rolls with higher spatial wavenumbers were observed.

(7) Good correlation was found between the flow visualization observations and the heat transfer data. Situations where the heat transfer did not scale, corresponded closely to those where the convection patterns were unsteady. Bent steady rolls appeared to have no effect on the heat transfer.

(8) The existence of the unsteady rolls, observed for certain values of Ra and ϕ, has been tentatively associated with a secondary instability caused by a shear instability on the observed upslope velocity components associated with the longitudinal rolls. Such a secondary instability seems to be subject to temporary suppression as evidenced by results at $\phi = 20°$ and 25°. This theory agrees qualitatively with the theory of Clever & Busse (1977).

Appendix. Details of the convective form study

This appendix contains a detailed analysis of the photographic results of figures 6–9, with a summary of associated observations.

For $Ra \simeq 1925$, photographs were taken at $\phi = 5°$, 10° and 15° (figure 6). Both figure 6(*a*) and (*b*) ($\phi = 15°$ and 10°) exhibit steady bent rolls. Figure 6(*c*) ($\phi = 15°$) exhibits wavy rolls. At $\phi = 15°$ the smoke detail was observed to slowly fade, suggesting a mildly unsteady situation; however, no lateral motion was observed. At $\phi = 17{\cdot}5°$ and 20° the smoke faded so rapidly that after 5 minutes a photograph was not possible. At $\phi = 20°$ the rolls, while fading, showed clean signs of lateral motion with occasional evidence of looping.

For $Ra \simeq 2425$, photographs were taken at $\phi = 5°$, 10°, 15°, 17·5° and 20° (figure 7). Figure 7(*a*) and (*b*) ($\phi = 5°$ and 10°) show rolls which are quite straight, with a slight bend near the top of the pictures. Figure 7(*c*) and (*d*) ($\phi = 15°$ and 17·5°) show straight rolls, although for $\phi = 17{\cdot}5°$ there is slight evidence of waviness. There was no indication of lateral motion in either case. Figure 7(*e*) ($\phi = 20°$) clearly exhibits wavy rolls. Although no lateral motion was observed in the layer, the smoke diffused rapidly. It is noted here that, as a general observation, when the smoke faded, the fading began at the hinged end of the apparatus and proceeded up the plates. At $\phi = 22{\cdot}5°$ there was clear indication of slow lateral motion and instances of looping. At $\phi = 25°$ these features were again observed, the motions being more rapid.

For $Ra \simeq 2960$, photographs were taken at $\phi = 5°$, 10°, 15°, 17·5°, 20° and 22·5° (figure 8). Figure 8(*a*) ($\phi = 5°$) shows the characteristic bent rolls. At $\phi = 10°$ (figure 8*b*), the bend is not so obvious. Figure 8(*c*), (*d*), (*e*), (*f*) ($\phi = 15°$, 17·5°, 20° and 22·5°) all show straight rolls with no sign of waviness. Upon inclining the layer to $\phi = 25°$, wavy rolls were clearly observed with the smoke totally diffused after 4 min. Upon reintroducing smoke, lateral motion with looping was observed. At $\phi = 27{\cdot}5°$ the motion was similar but more severe.

For $Ra \simeq 4050$, photographs were taken at $\phi = 5°$, 15°, 17·5° and 20° (figure 9). For $\phi = 5°$ (figure 9*a*) the rolls appear quite straight. The $\phi = 15°$, 17·5° and 20° photographs (figure 9*b*, *c*, *d*) all exhibit steady straight rolls. At $\phi = 22{\cdot}5°$, gentle lateral motion was observed. As well, the rolls tended to alternately thin and thicker, with an appearance similar to that observed when a series of marbles is forced through an undersized flexible tube. At $\phi = 25°$ and 27·5°, the rolls were very unsteady with evidence of looping.

For $Ra \simeq 5000$, no photographs were taken. However, at $\phi = 15°$, 17·5° and 20°,

the usual steady straight rolls were observed. At $\phi = 22{\cdot}5°$, the rolls were observed to loop, dispersing the smoke within a few minutes. At $\phi = 25°$ and $27{\cdot}5°$, highly unsteady rolls were observed.

For $Ra \simeq 5800$, the $\phi = 5°$ and $10°$ rolls were straight and steady; however, at $\phi = 15°$ there were clear signs of a slow lateral motion. At $\phi = 17{\cdot}5°$, waviness and lateral motion were clearly observed. For $\phi = 20°$ and $22{\cdot}5°$, the rolls were very unsteady with rolls looping.

The observations of this appendix are summarized in figure 10.

This work was supported by an operating grant from the National Research Council of Canada. In addition, the first author was supported by a National Research Council of Canada Post-Graduate Scholarship. Both grants are acknowledged with gratitude. The authors would like to thank Dr F. H. Busse and Dr R. M. Clever for providing an expanded version of their results which made detailed comparisons with their work possible.

REFERENCES

Birikh, R. V., Gershuni, G. Z., Zhukhovitskii, E. M. & Rudakov, R. N. 1968 Hydrodynamic and thermal instability of a steady convective flow. *Prikl. Math. Mech.* **32**, 256–263.

Clever, R. M. 1973 Finite amplitude longitudinal convection rolls in an inclined layer. *Trans. A.S.M.E.* C, *J. Heat Transfer*, **95**, 407–408.

Clever, R. M. & Busse, F. H. 1977 Instabilities of longitudinal convection rolls in an inclined layer. *J. Fluid Mech.* **81**, 107–127.

De Graff, J. G. & Van der Held, E. F. M. 1953 The relation between the heat transfer and the convection phenomena in enclosed plane air layers. *Appl. Sci. Res.* A, **3**, 393–409.

Gershuni, G. Z. & Zhukhovitskii, E. M. 1969 Stability of plane-parallel convective motion with respect to spatial perturbations. *Prikl. Math. Mech.* **33**, 855–860.

Hart, J. E. 1971*a* Stability of the flow in a differentially heated inclined box. *J. Fluid Mech.* **47**, 547–576.

Hart, J. E. 1971*b* Transition to a wavy vortex regime in convective flow between inclined plates. *J. Fluid Mech.* **48**, 265–271.

Hollands, K. G. T. 1965 Convectional heat transfer between rigid horizontal boundaries after instability. *Phys. Fluids* **8**, 389–390.

Hollands, K. G. T. 1967 Natural convection in a horizontal layer of air with internal constraints. Ph.D. thesis, McGill University.

Hollands, K. G. T. & Konicek, L. 1973 Experimental study of the stability of differentially heated inclined air layers. *Int. J. Heat Mass Transfer*, **16**, 1467–1476.

Hollands, K. G. T., Unny, T. E., Raithby, G. D. & Konicek, L. 1976 Free convective heat transfer across inclined air layers. *Int. J. Heat Mass Transfer*, **98**, 189–193.

Konicek, L. 1971 Experimental determination of critical Rayleigh numbers and heat transfer through horizontal and inclined air layers. M.A.Sc. thesis, University of Waterloo.

Kursweg, U. H. 1970 Stability of natural convection within an inclined channel. *Trans. A.S.M.E.* C, *J. Heat Transfer*, **92**, 190–191.

Malinov, A. V. 1971 Experimental study of natural convection in differently oriented slotted cavities. *Soviet Res. Heat Transfer*, **3**, 193–199.

Platzman, G. W. 1965 The spectral dynamics of laminar convection. *J. Fluid Mech.* **23**, 481–510.

Unny, T. E. 1972 Thermal instability in differentially heated inclined fluid layers. *Trans. A.S.M.E.* E, *J. Appl. Mech.* **39**, 41–46.

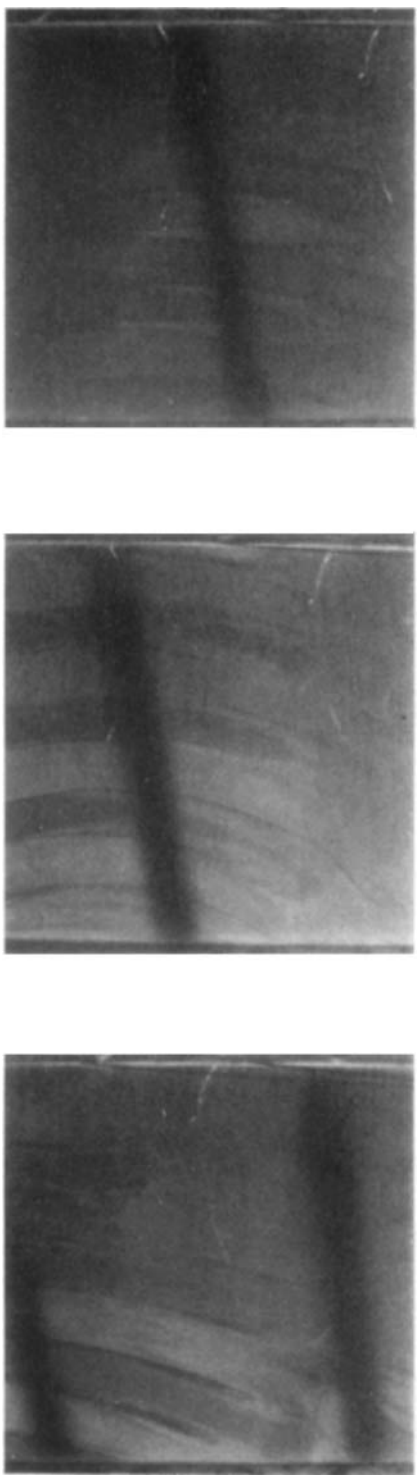

(*c*)

(*b*)

(*a*)

FIGURE 6. Convection patterns for $Ra \simeq 1925$. (*a*) $\phi = 5°$; (*b*) $\phi = 10°$; (*c*) $\phi = 15°$.

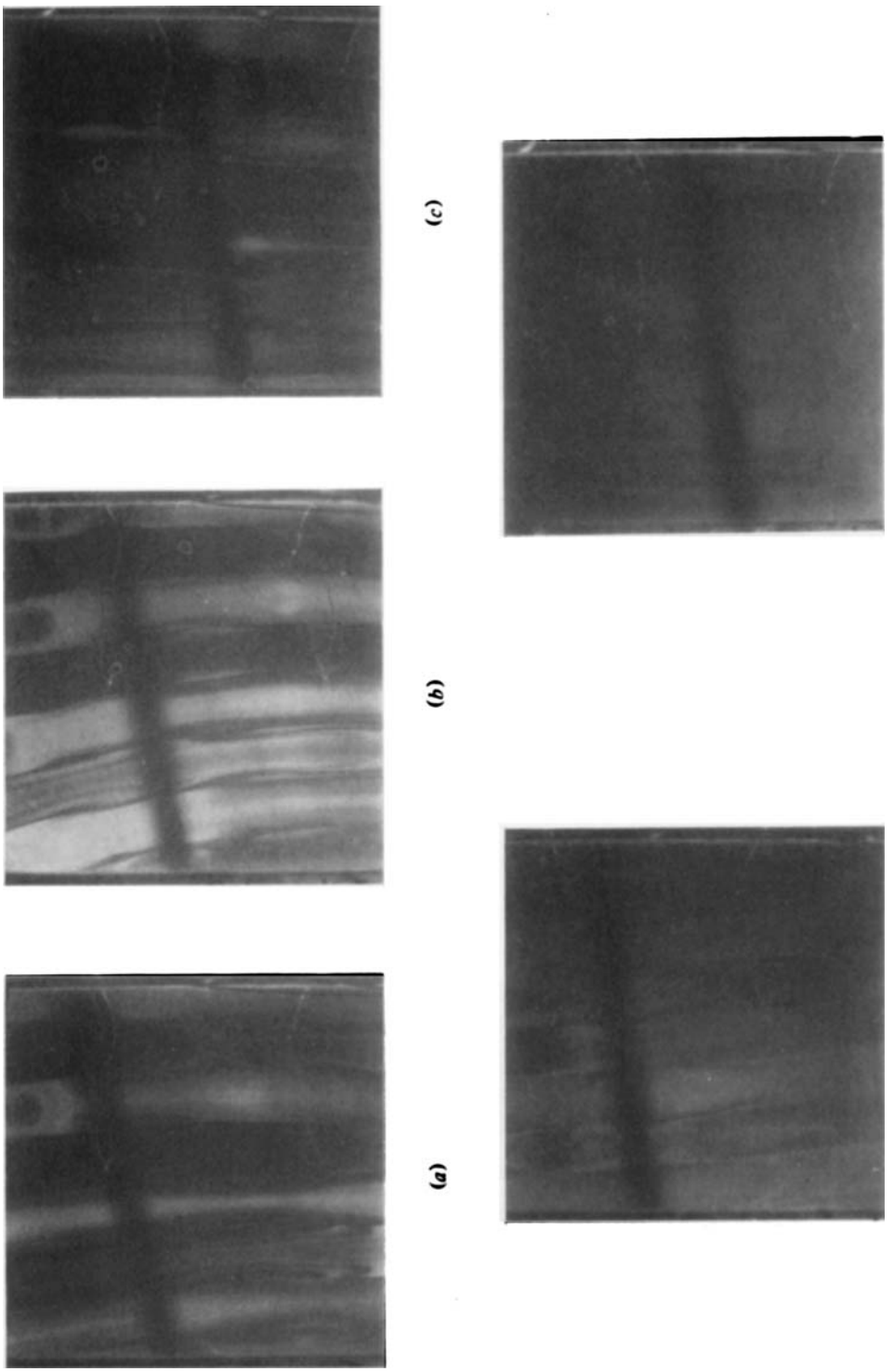

FIGURE 7. Convection patterns for $Ra \simeq 2425$. (*a*) $\phi = 5°$; (*b*) $\phi = 10°$; (*c*) $\phi = 15°$; (*d*) $\phi = 17{\cdot}5°$; (*e*) $\phi = 20°$.

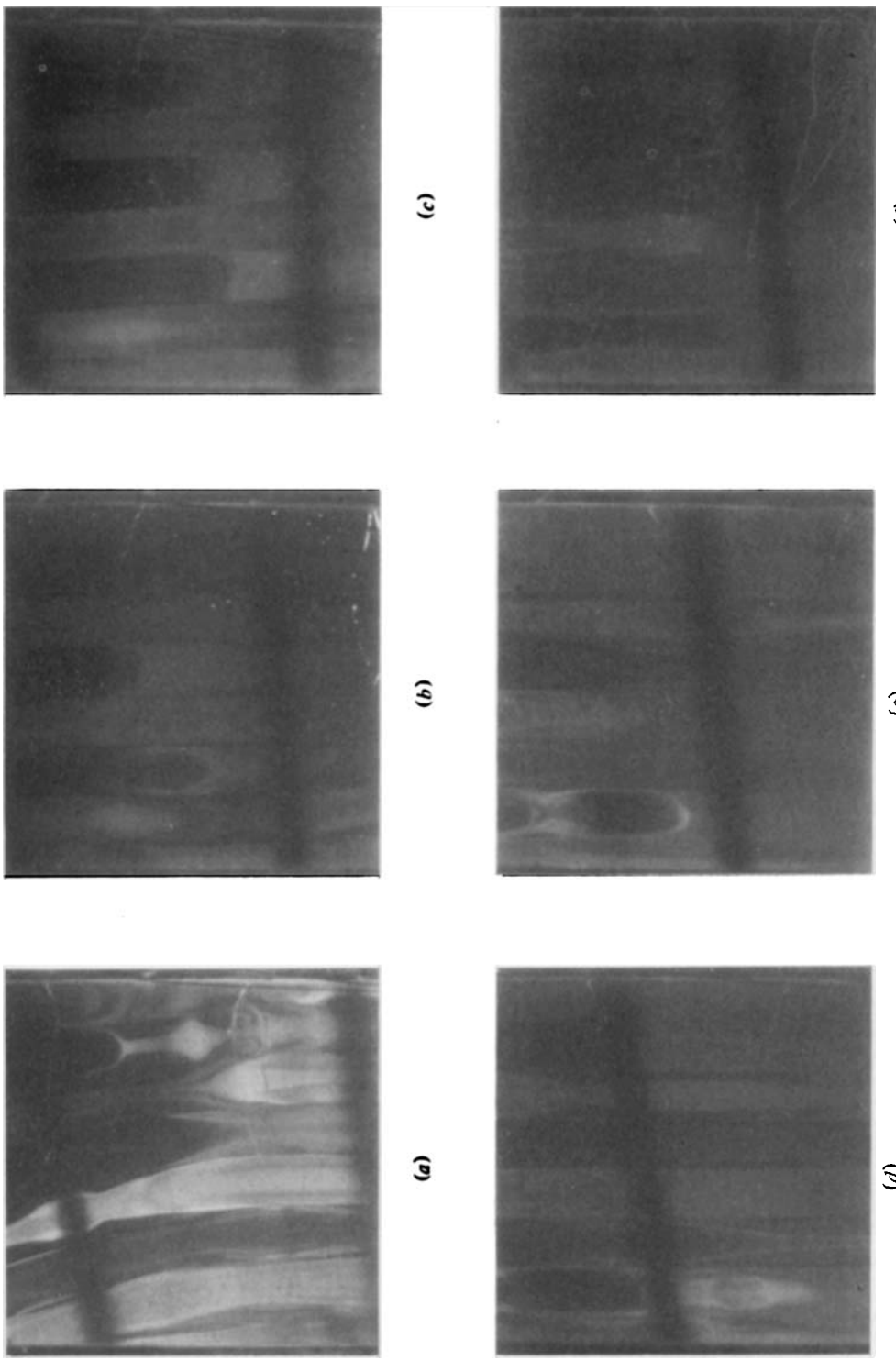

FIGURE 8. Convection patterns for $Ra \simeq 2960$. (*a*) $\phi = 5°$; (*b*) $\phi = 10°$; (*c*) $\phi = 15°$; (*d*) $\phi = 17{\cdot}5°$; (*e*) $\phi = 20°$; (*f*) $\phi = 22{\cdot}5°$.

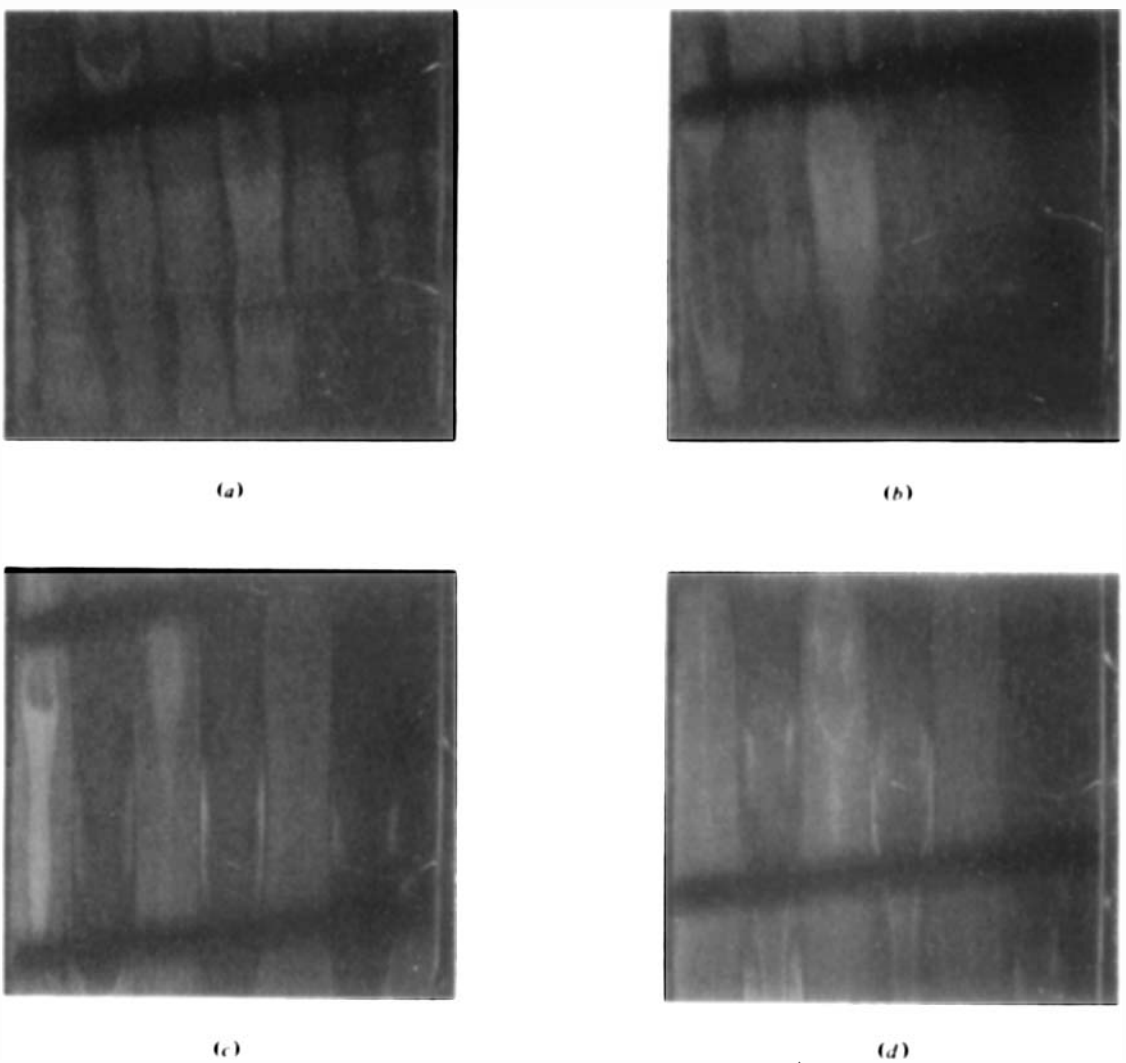

FIGURE 9. Convection patterns for $Ra \simeq 4050$. (*a*) $\phi = 5°$; (*b*) $\phi = 15°$; (*c*) $\phi = 17{\cdot}5°$; (*d*) $\phi = 20°$.

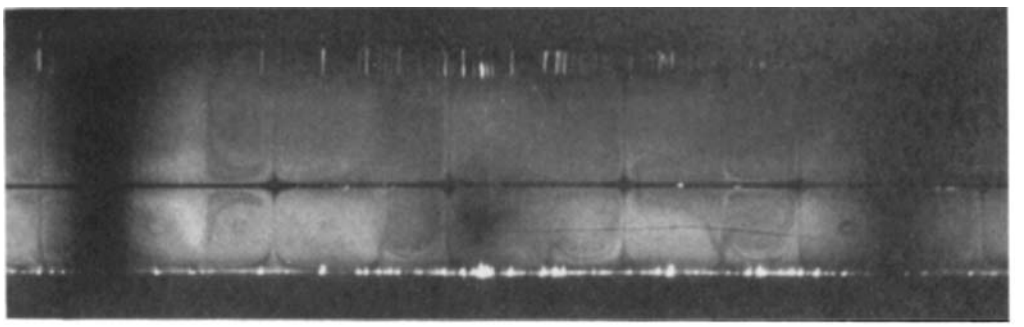

(*a*)

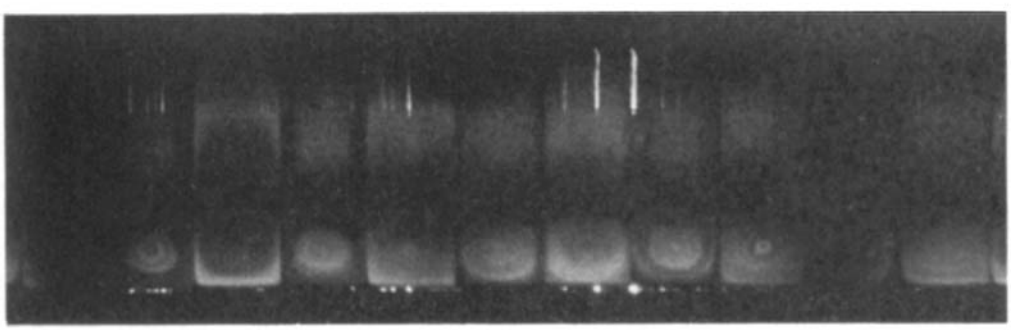

(*b*)

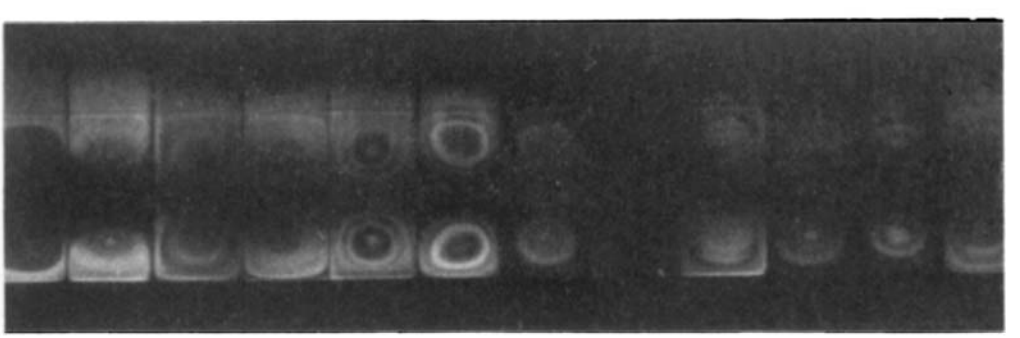

(*c*)

FIGURE 11. For legend see overleaf.

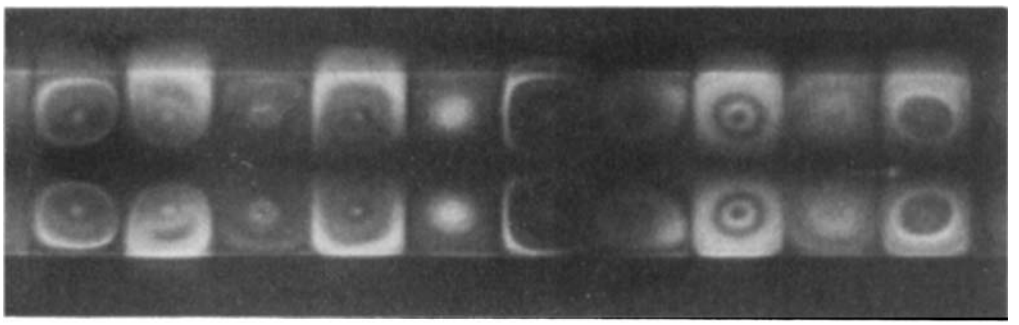

(*d*)

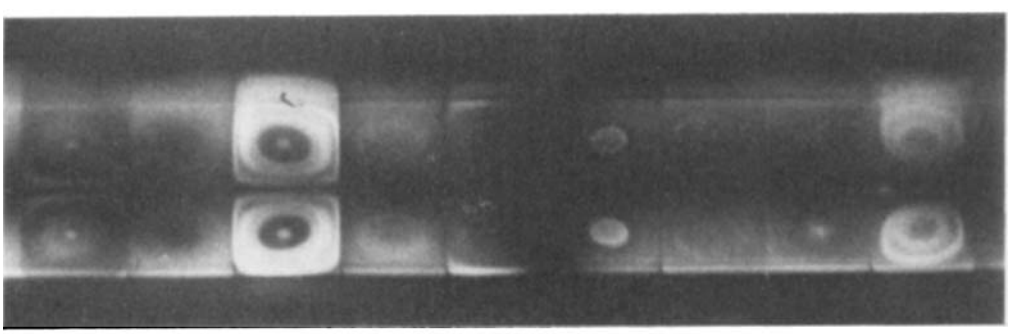

(*e*)

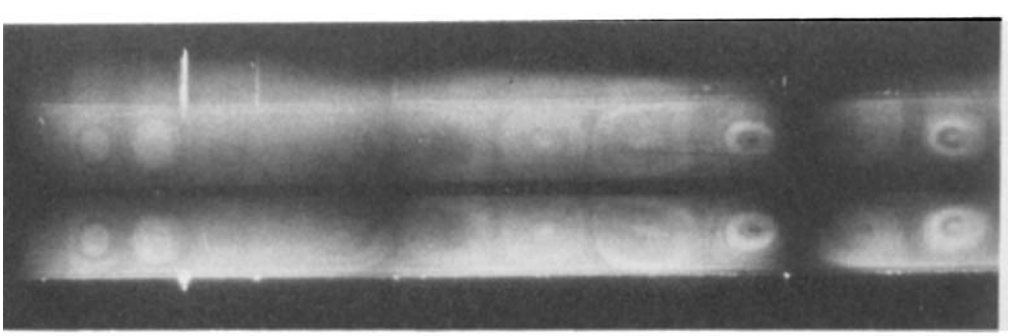

(*f*)

FIGURE 11. Cross-sectional view of rolls ($\phi = 15°$). (*a*) $Ra \simeq 1925$; (*b*) $Ra \approx 2370$; (*c*) $Ra \approx 2625$; (*d*) $Ra \approx 2950$; (*e*) $Ra \approx 3870$; (*f*) $Ra \approx 5080$.

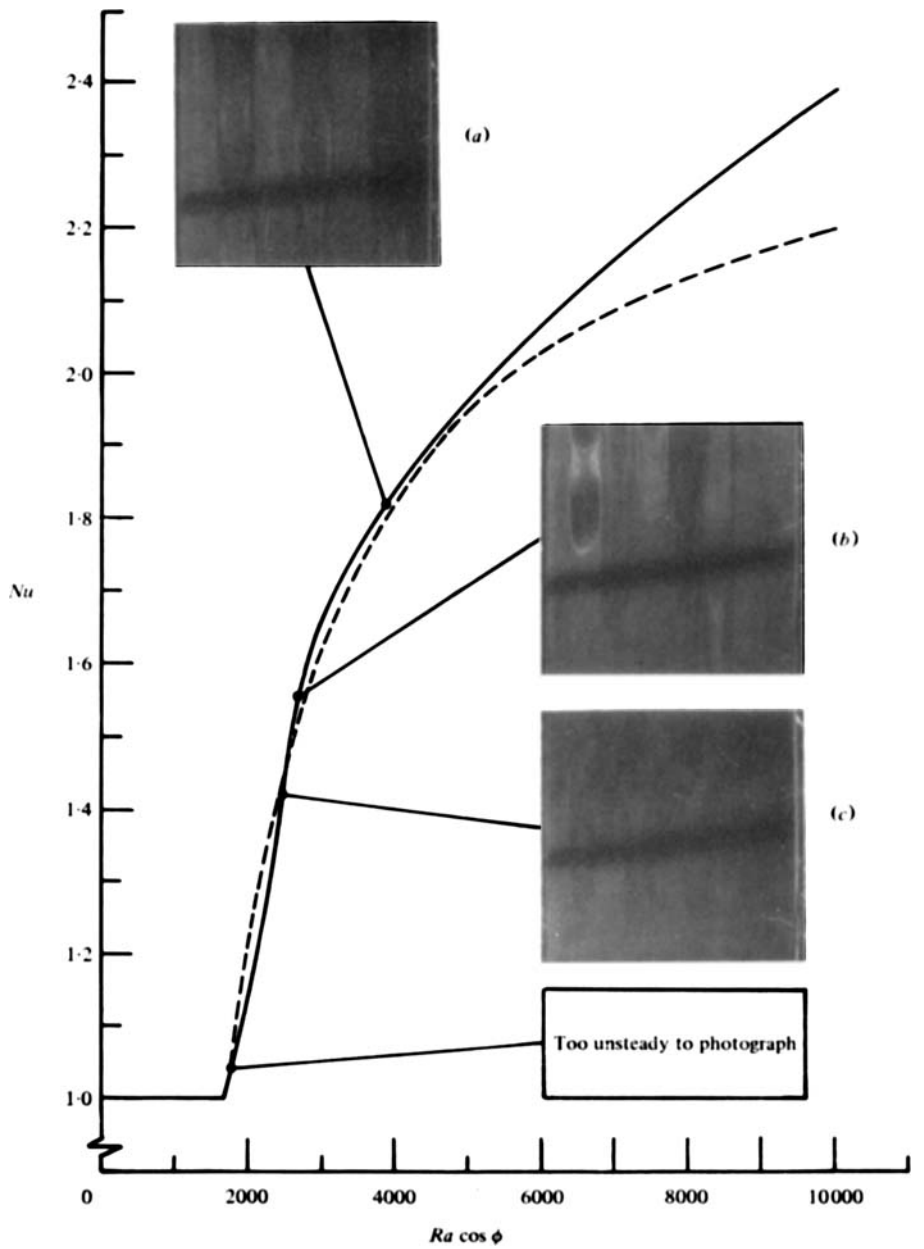

FIGURE 13. The flow regimes at $\phi = 20°$. ——, measured heat transfer; – – –, equation (4). (*a*) Steady, $a \approx 2{\cdot}58$; (*b*) steady, $a \approx 3{\cdot}05$; (*c*) marginally unsteady, $a \approx 3{\cdot}60$.